A.J. Fenn

Near-Field Testing of Adaptive Radar Systems

Large phased-array antennas with multiple displaced phase centers are applied to radar applications that require adaptive suppression of jamming and clutter. Before the deployment of this adaptive radar, tests must verify how well the system detects targets and suppresses clutter and jammer signals. This article discusses a recently developed focused near-field testing technique that is suitable for implementation in an anechoic chamber. With this technique, phased-array near-field focusing provides far-field equivalent performance at a range distance of one aperture diameter from the adaptive antenna under test. The technique is applied theoretically to a dual-phase-center sidelobe-canceler antenna with multiple near-field sources within the main beam and sidelobes. Numerical simulations indicate that near-field and far-field testing can be equivalent.

The development of any radar system requires tests of the associated hardware and software at various levels of the design. Before a radar system can be deployed, design specifications must be verified at the subsystem development level, system prototype level, and final system level. For ground-based or airborne radar systems, the final system can be tested in the field and modified or upgraded as necessary. For a spaceborne radar, however, where the deployed system hardware is not accessible, comprehensive prelaunch testing and modifications must be performed on the ground. This article describes a recently developed focused near-field technique that measures the performance characteristics of adaptive radar systems within a ground-test facility. Although the technique is especially suitable for space-based radar systems [1–3], it applies to most adaptive ground-based and airborne radar systems and communications systems as well.

The important subsystems of an adaptive radar system consist of an antenna, a multichannel receiver, and a signal processor. The radar receives desired target signals along with interference consisting of noise, background clutter, and sidelobe jamming (Fig. 1). The antenna collects signals that the receiver filters, downconverts, and digitizes. The digitized data are then processed by the signal processor, which suppresses undesired interference signals and produces desired target reports.

The radar system typically utilizes a deployable planar phased-array antenna structure with a largest dimension of 10 to 50 m and a nominal operating range of several thousand kilometers. Because of this long operating range, the antenna receives planar-shaped wavefronts from targets, clutter, and jamming. To approximate plane-wavefront conditions at microwave frequencies, a conventional far-field test distance is on the order of 2 to 10 km. The minimum far-field distance is determined by $2D^2/\lambda$, where D is the antenna diameter and λ is the wavelength. For low-sidelobe antenna pattern measurements, a longer far-field minimum test distance is often used. It is difficult if not impossible to place many radiating test sources on a far-field ground-test range over a wide field of view, and demonstrate low sidelobes together with jammer/clutter suppression. Thus an alternate ground-test configuration is necessary. Near-field testing, with the radar system positioned in a high-quality controlled-environment anechoic chamber, is a desirable method for evaluating radar system performance. Figure 2 shows the proposed test method. The antenna and test sources (jammer,

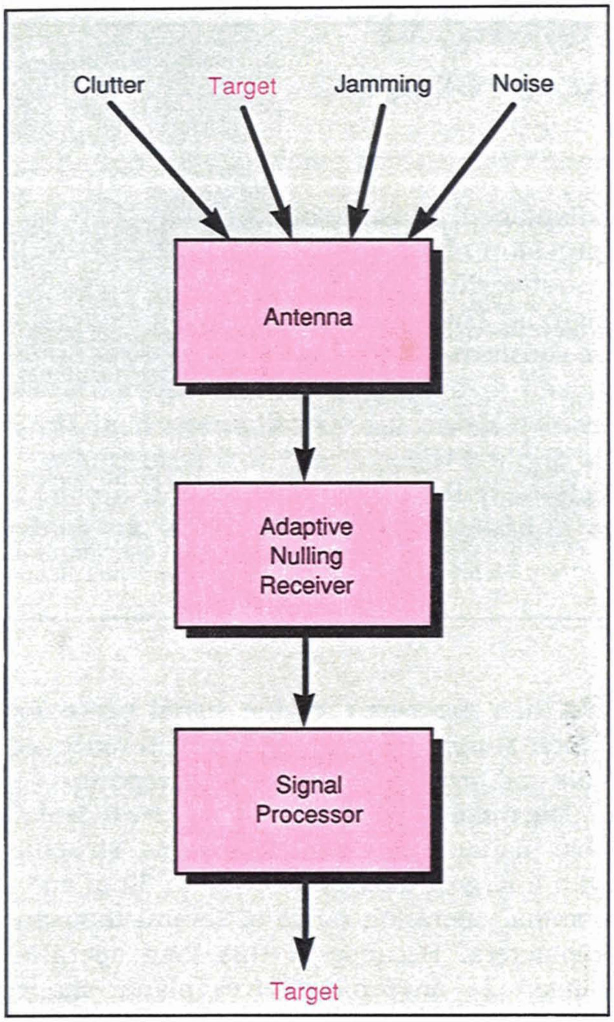

Fig. 1—The important subsystems of an adaptive radar system. Noise, clutter, jamming, and desired target signals are received by the antenna. These signals are downconverted and digitized by the receiver and then processed within the signal processor to provide desired target information.

clutter, and target) are placed within the anechoic chamber, and the adaptive nulling receiver and signal processor are placed outside the anechoic chamber. The details of how this technique naturally develops are described below.

Figure 3 depicts the various regions in front of a test antenna. The horizontal axis is the antenna dimension D/λ and the vertical axis is the normalized test distance z/D. The figure indicates the far-field test region, but this region is not considered for potential testing for the size reasons cited above. Planar scanning with a probe antenna at a distance of a few wavelengths (typically 3λ) from the test antenna is a conventional near-field technique for calibration and far-field radiation pattern measurement [4, 5]. This form of planar near-field scanning is a non-real-time measurement technique in which near-field data are collected and far-field data are computed. However, an adaptive nulling test requires real-time signal wavefronts, which precludes using the planar near-field scanning technique. The Fresnel region [6] (or transition region between the near field and far field), which extends from about $0.6\sqrt{D^3/\lambda}$ to $2D^2/\lambda$, offers reduced-range testing but is still too distant for large antennas. Ranges less than $0.6\sqrt{D^3/\lambda}$ define the near-field region.

A compact-range reflector [7] can reduce the test distance to two to four aperture diameters ($2D$ to $4D$), which is within the near-field region. This technique utilizes a parabolic reflector to convert the spherical wavefront from a feed horn into a planar wavefront. A compact-range reflector can be used for adaptive nulling tests provided that the wavefront is sufficiently free of multipath. The required reflector diameter is large, however (approximately $2D$ at L-band frequencies and below), and sources widely spaced in the test-antenna field of view are difficult to achieve. Thus the compact-range reflector is also not of interest here. All of the above techniques create plane-wave illumination for the antenna, which results in impractical test geometries for adaptive nulling. To develop a suitable testing method, the plane-wave constraint must be dropped and spherical waves must be considered instead.

A recently developed technique called focused near-field adaptive nulling implements conventional near-field focusing to establish an instantaneous or real-time antenna radiation pattern that is equivalent to its far-field pattern [8]. This technique appears to be ideal for ground-based testing. The test distance varies from one to two aperture diameters (D to $2D$) of the adaptive antenna under evaluation, as shown in Fig. 3. For large antenna diameters this test distance is located well within the near-field boundary. The incident wavefront from

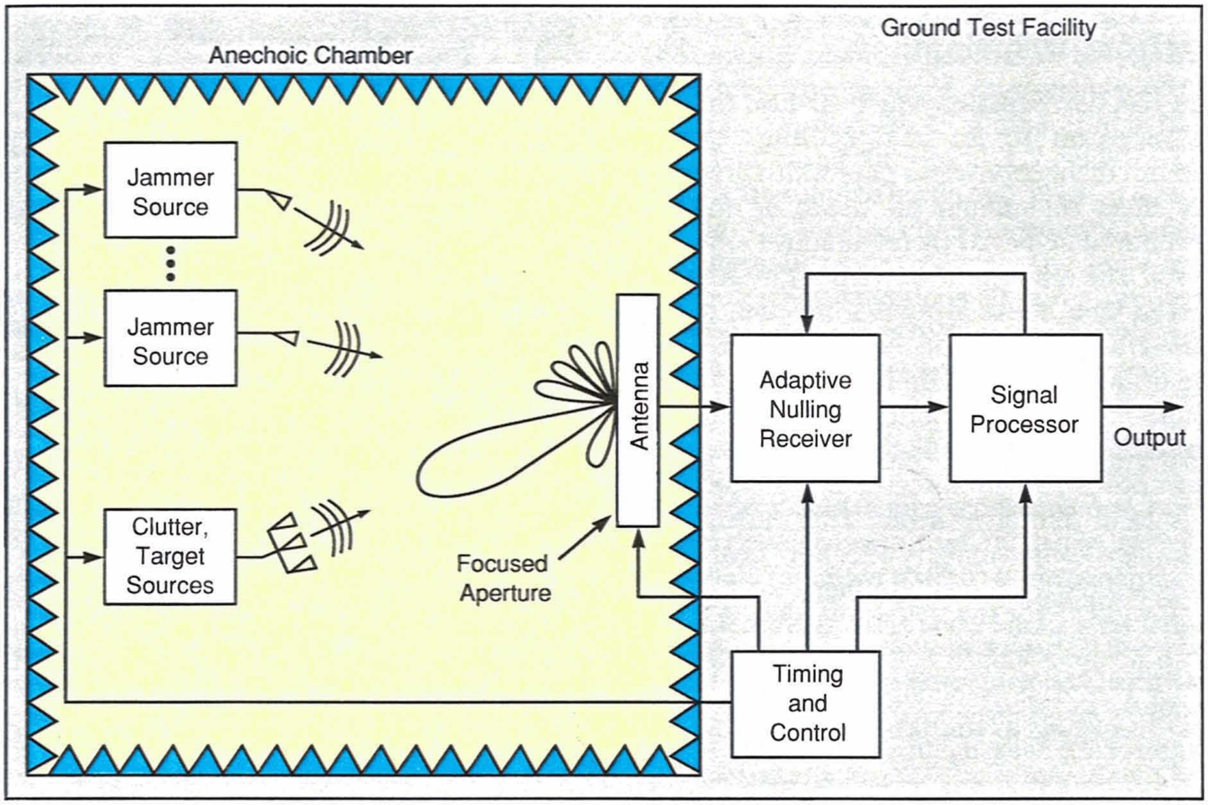

Fig. 2—Focused near-field nulling concept for a ground test of an adaptive radar system. The antenna under test and radiating sources (clutter, jammer, targets) are positioned within a high-quality anechoic chamber. Focusing the test antenna in the near field produces conditions equivalent to the far field. By utilizing proper timing and control, a signal environment comparable to fielded-radar system conditions can be achieved. The adaptive nulling receiver and signal processor operate in real time. This configuration provides a thorough test of the important radar subsystems.

radiating sources in the near field is spherical rather than planar, which allows the radiating source antennas to be simple horns or dipoles. Four principal papers describing focused near-field adaptive nulling have been published by the author [8–11]. The equivalence between conventional far-field adaptive nulling and focused near-field adaptive nulling has been demonstrated for sidelobe canceler [8] and fully adaptive arrays [9]. Near-field clutter and jamming for a sidelobe canceler have also been addressed [10]. In Refs. 8 through 10, the analysis assumes that the array elements and radiating sources are isotropic. Reference 11 studies the effects of array polarization and mutual coupling, and demonstrates that the equivalence between near-field and far-field adaptive nulling still holds for single and multiple jammers. The present article expands the mutual coupling formulation to include clutter and jamming.

In the next section the characteristics of an incident signal wavefront are investigated as a function of source distance and angle of arrival. This investigation is followed by a description of how focusing is used to establish appropriate quiescent conditions for near-field adaptive nulling. An application of the technique to a displaced phase-center antenna (DPCA) is made, and details of the theoretical formulation are given. Antenna modeling is accomplished by using the method of moments, including array mutual-coupling effects. The theory is applied to a linear array of dipole elements with dipole near-field sources (clutter and jamming). The results show that focused near-field adaptive nulling is a viable approach to testing full-scale adaptive radar systems.

Near-Field/Far-Field Source Wavefront Dispersion

This section explains why near-field nulling can be equal to far-field nulling. Signal wavefront dispersion (time-bandwidth product) is an effect that limits the depth of null (or cancellation) achieved by an adaptive antenna [12, 13]. The amount of wavefront dispersion γ observed by a linear array is a function of the bandwidth, array length, source range, and angle of incidence. A simple but effective dispersion model for spherical-wave incidence and plane-wave incidence considers the wavefront dispersion observed across the endpoints of an adaptive array. This calculation gains some initial insight into how near-field nulling relates to far-field nulling.

Consider a plane wave arriving from infinity and an array of length L. The far-field dispersion for this case is denoted γ_{FF} and is computed according to the product of bandwidth and time delay as

$$\gamma_{FF} = \frac{BL}{c} \sin \theta_i \tag{1}$$

where B is the nulling bandwidth, c is the speed of electromagnetic wave propagation, and θ_i is the angle of incidence. Note that the dispersion is maximum for endfire incidence ($\theta_i = 90°$) and zero for broadside incidence ($\theta_i = 0°$). Next, consider a point source at a constant distance $z = z_i$ and variable angle $\theta = \theta_i$, which produces an incident spherical wavefront. The distances between the source and the two endpoints are denoted r_1 and r_2. The near-field dispersion γ_{NF} is given by

$$\gamma_{NF} = \frac{BL}{c} \frac{(r_1 - r_2)}{L} \tag{2}$$

where the quantity $(r_1 - r_2)/L$ is the normalized range difference. Equations 1 and 2 show that the far-field and near-field dispersions have a common factor BL/c. If near-field nulling is

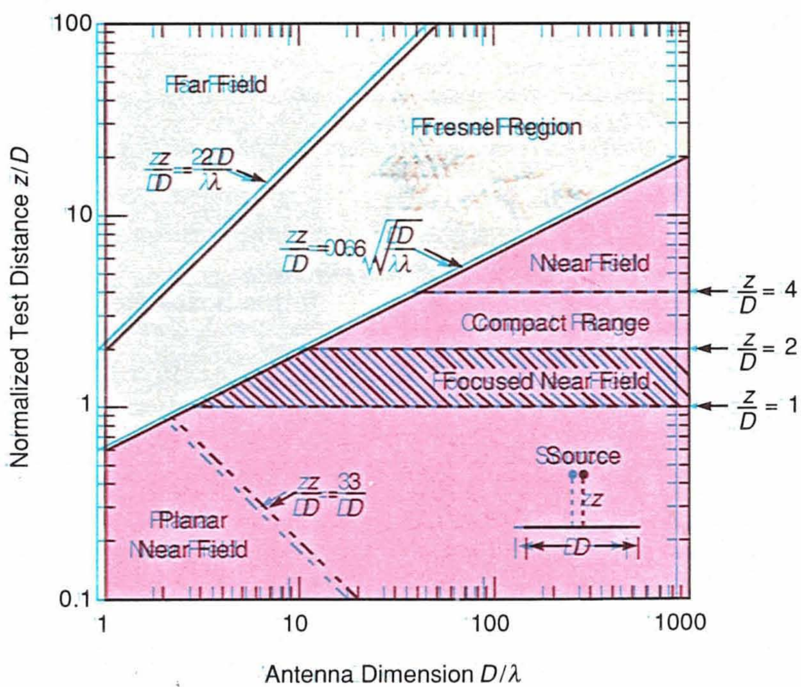

Fig. 3—Summary of antenna test regions. The hemispherical volume in front of an antenna can be divided into a number of test regions. The three basic regions are far field, Fresnel, and near field. The near-field region (shown in red) can be further divided into compact range (a reflector-based method), focused near field (which is addressed in this article), and planar near field. The focused near-field region is located between one and two aperture diameters from the antenna under test.

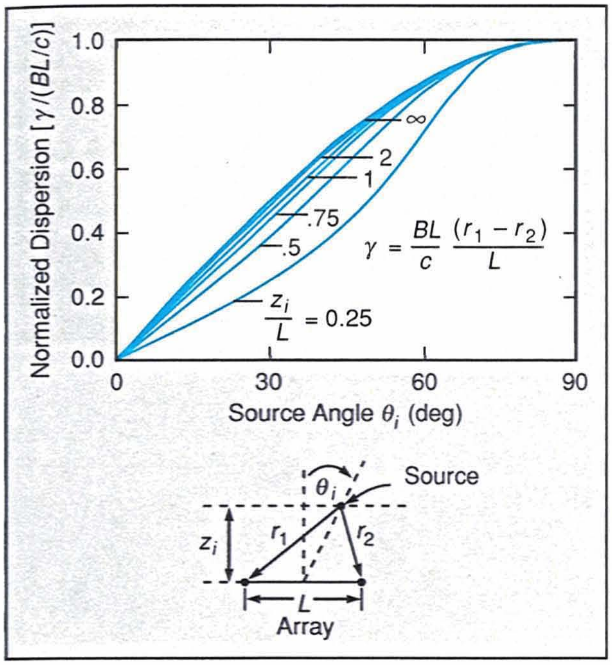

Fig. 4—Normalized wavefront dispersion as a function of source angle of arrival. The wavefront dispersion (time-bandwidth product), observed relative to the end points of an antenna, is a simple but effective model for comparing the characteristics of near-field and far-field sources. Maximum dispersion occurs when the source (either near field or far field) illuminates the antenna from endfire ($\theta_i = 90°$). For source distances of one aperture diameter or more, the difference between the near-field and far-field dispersion is small.

possibly equivalent to far-field nulling, then γ_{FF} must be equivalent to γ_{NF}. This condition is clearly satisfied when $(r_1 - r_2)/L = \sin\theta_i$. Figure 4 shows a plot of the normalized dispersion $\gamma/(BL/c)$ as a function of the angle of incidence for values of source distance from 0.25 to 2 aperture lengths (i.e., the normalized source distance is varied from z/L = 0.25 to 2). This figure shows that the near-field dispersion approaches the value of the far-field dispersion for source distances greater than approximately one aperture diameter, or $z/L = z/D \geq 1$ (in this article, aperture length L and aperture diameter D are equivalent and interchangeable). At one diameter, the percent difference between near-field and far-field dispersion is less than 10%. At two diameters, the percent difference is less than 3%. Clearly, at source distances such that $z/D \geq 0.5$ (one-half aperture diameter), the near-field dispersion is significantly different (by as much as 30%) compared to the far-field dispersion.

At source distances of one to two aperture diameters, the incident near-field wavefront dispersion appears to be comparable to that of a far-field wavefront. However, before the radar system attempts to perform near-field adaptive nulling, the receive-antenna quiescent conditions must be made to appear the same as far-field quiescent conditions. This requirement is achieved by focusing the antenna under test as described in the next section.

Focused Near-Field Testing Concept

The near-field testing technique described in this article assumes that the array quiescent near-field radiation pattern has the same characteristics as the quiescent far-field radiation pattern. This assumption requires the formation of a main beam and sidelobes in the near field. The dynamic range of received signals from sources distributed across the radar field of view depends upon the antenna quiescent conditions. Phase focusing can be used to produce an array near-field pattern that approximately equals the far-field pattern [14].

Figure 5 shows a continuous wave (CW) calibration source located at a desired focal point of the array. The array maximizes the signal received from the calibration source by adjusting its phase shifters so that the spherical wavefront phase variation is removed. The first step to determine this adjustment is to choose a reference element; this reference is usually the center element of the array. The voltage received at the nth array element relative to the center element of the array is computed in this article by using the method of moments [15]. To maximize the received voltage at the array output, the phase conjugate of the incident wavefront must be applied at the array elements. The resulting instantaneous array radiation pattern seen at the source test plane $z = z_o$ looks similar to a far-field pattern [11]. In this pattern a main beam points at the array focal point, and sidelobes exist at angles away from the main beam. Interferers are then placed on near-field sidelobes in the test (or focal) plane, as shown in Fig. 5. Similarly,

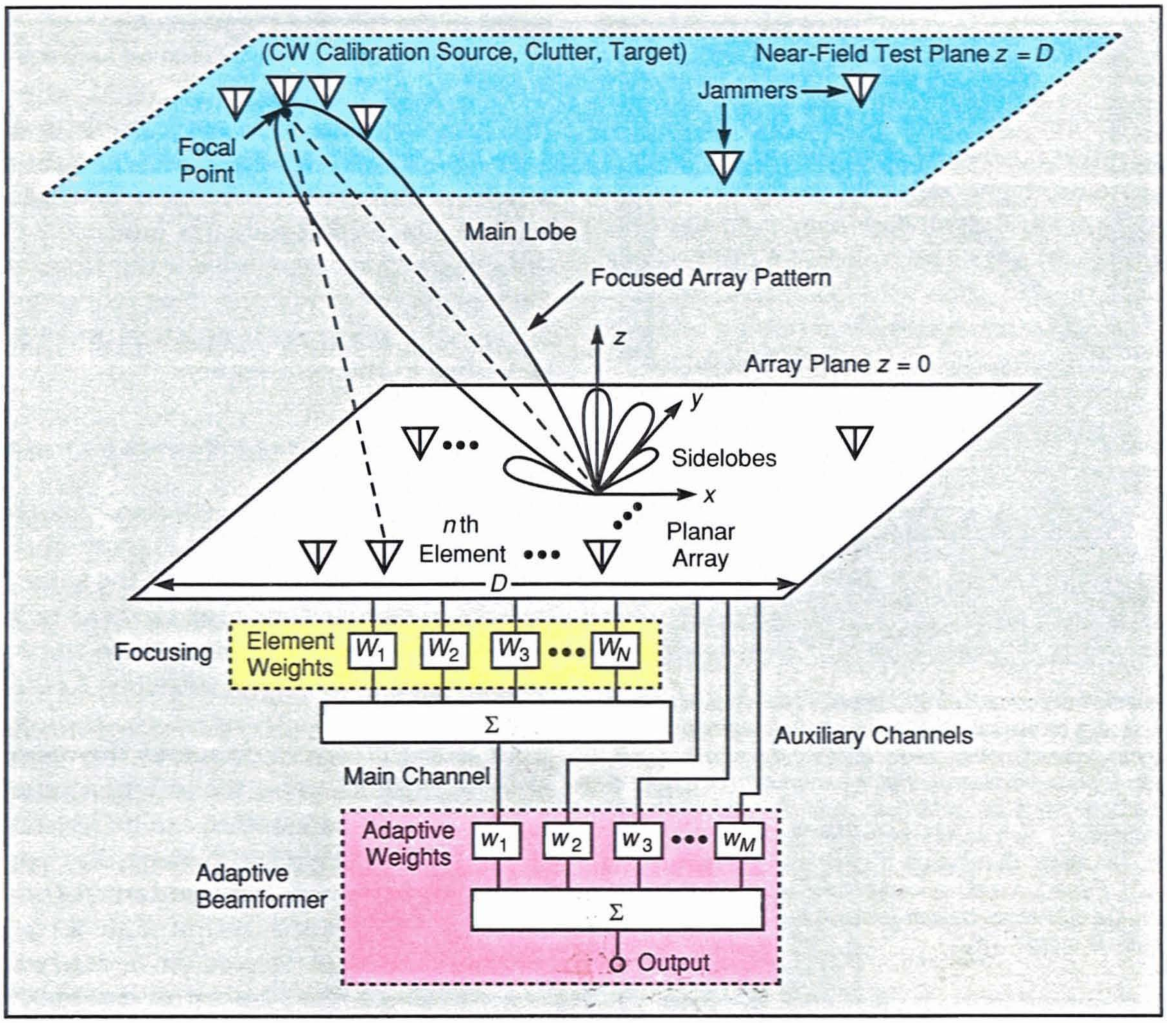

Fig. 5—Focused near-field adaptive nulling test concept. A CW radiating source is used as a calibration signal for a phased-array antenna. The antenna-element phase shifters focus the receive antenna radiation pattern in the direction of the calibration source. This focusing creates an antenna radiation pattern that is similar to a far-field radiation pattern. Clutter and target sources can be placed on the main beam as desired. Similarly, jammers can be positioned on sidelobes.

clutter sources are positioned on the near-field main beam. Near-field focusing that uses only phase control results in some distortion of the main beam and first sidelobes. Amplitude control can make the near-field pattern main beam and first sidelobes more closely resemble a far-field pattern [16]. For simplicity, this article describes phase focusing only.

The minimum size of the required ground-test facility can be determined by considering the near-field geometry. For compatibility with conventional planar near-field scanning equipment, a flat test plane is assumed. Let θ_{max} denote the maximum angle of interest for the antenna radiation pattern. The required near-field scan length D_x for pattern coverage of $\pm\theta_{max}$ is given in terms of the F/L ratio as

$$D_x = 2L\left(\frac{F}{L}\right)\tan\theta_{max}\,.$$

Figure 6 depicts the required scan lengths for 60° and 120° field-of-view coverage with F/L ratios of L and $2L$. To reduce the scan length (or source deployment length) the F/L ratio must be kept as close to unity as possible. Clearly, the ground-test facility must be large enough to encompass both the desired scan length D_x and the focal length F.

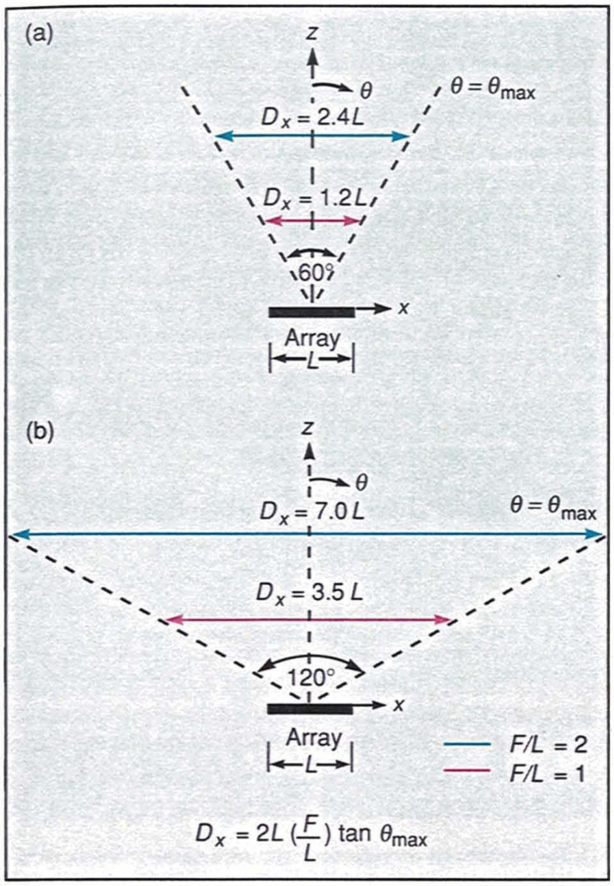

Fig. 6—Examples of source deployment and scan length D_x for (a) 60° field of view and (b) 120° field of view. These figures illustrate the importance of a close test distance.

The application of the focused near-field testing concept to a specific radar system requires the following important assumptions:

(1) the incident near-field wavefront must be reasonably well matched to a far-field wavefront;
(2) the adaptive antenna under test must be focused at the range of the test sources;
(3) the antenna characteristics, beamformer characteristics, and receiver characteristics, such as channel mismatch, must be independent of the type of wavefront (near field or far field); and
(4) the technique must be applicable to both analog and digital adaptive nulling systems.

The analysis in this article accounts for assumptions 1, 2, and part of 3 (antenna characteristics). The remaining assumptions, which are not expected to limit the technique, are not analyzed here.

Adaptive DPCA Radar

The DPCA technique can be applied to airborne or spaceborne radar systems that require adaptive suppression of jamming and clutter [2]. A DPCA array cancels stationary ground clutter from a moving platform by employing two or more independent receive phase centers with well-matched main beams. Figure 7 shows a moving target and a moving radar in a two-phase-center DPCA system. On transmit, the full aperture of the array sends a burst of pulses; on receive, two displaced portions of the aperture record the returned signals. Because of the platform motion, two consecutive transmit pulses occur corresponding to the transmit phase-center positions A_T and B_T. The radar transmit signal illuminates both moving targets and fixed ground terrain that, because of the radar cross section, produces the desired signals and clutter. Ground-based emitters also represent a source of interference or jamming.

On reception, the antenna phase-center displacement between the two receive apertures is adjusted to compensate for the platform velocity. For two transmit pulses separated in time by one pulse-repetition interval (PRI), the first reception occurs at the forward receive phase-center position, denoted A in Fig. 7. A second reception occurs at the trailing receive phase-center position B. This bistatic radar system is equivalent to a monostatic radar system that makes two independent observations of the signal environment at a single point in space. This common point, denoted AB, is located at the midpoint of the line joining either points A_T and A or B_T and B. During a PRI, the target moves while the clutter is effectively stationary. As a result, the target produces a relative phase shift during this time, while the clutter has no phase shift. The clutter is assumed to be correlated between the two phase centers. In contrast, wideband noise jamming is assumed to be uncorrelated between the two phase centers due to the one-PRI delay imposed in the signal processing. When the signals received by the two phase centers are adaptively combined, the

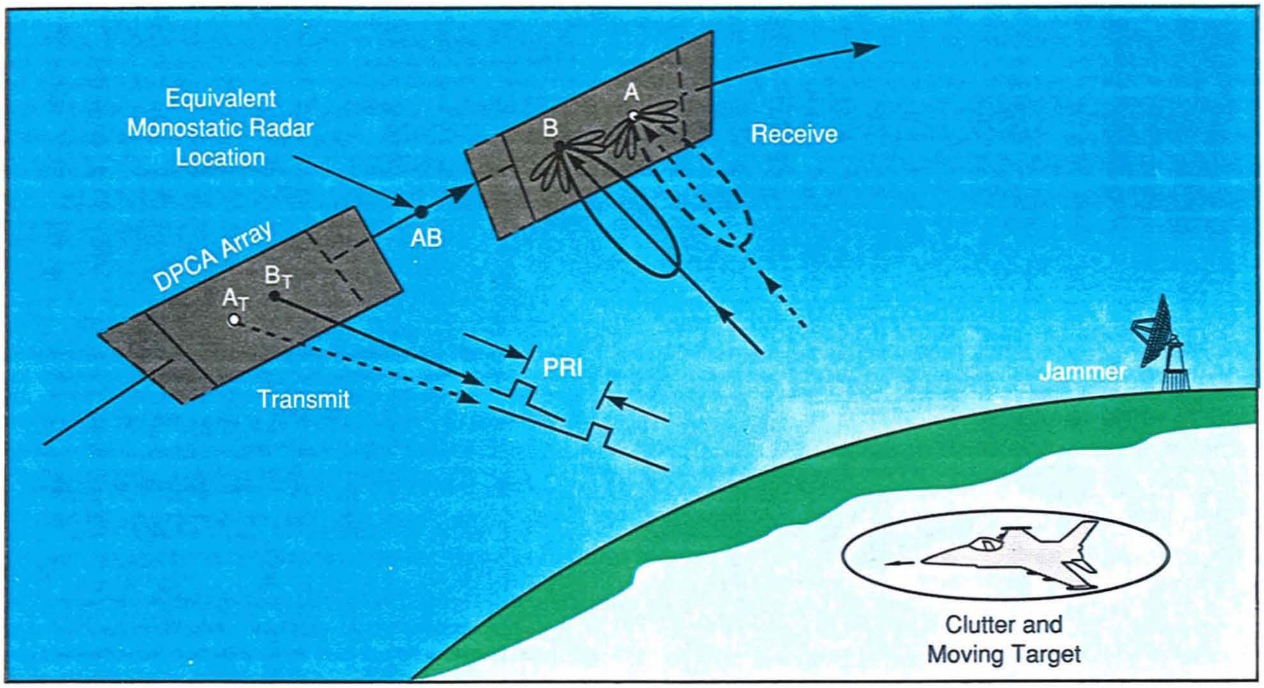

Fig. 7—Displaced phase-center antenna (DPCA) radar system concept. Receive phase centers (or subarrays) A and B compensate for the radar motion by creating a phase-center displacement. To cancel stationary main-beam clutter and sidelobe jamming, and to detect the target, the radar system effectively makes two measurements of the signal environment at the common point AB and adaptively combines the phase centers.

clutter and jammer are significantly canceled. The corresponding target signal depends on the amount of target phase shift during one PRI interval (0° phase shift produces no target signal while 180° phase shift produces maximum target signal). The DPCA quiescent main-beam pattern match is a function of array geometry and scan conditions (due to array-element mutual coupling), and hardware tolerances (such as the quantization and random errors of the transmit/receive [T/R] modules). Both T/R module effects and array mutual coupling are taken into account in the next two sections of this article.

Adaptive DPCA Array Formalism

Consider the DPCA array and adaptive beamformer as shown in Fig. 8. The array contains N elements that form the receive main channel. Included within these elements is a guard band of passively terminated elements that provides impedance matching to the active elements and isolation from ground-plane edges. The output from each of the array elements is first split into two paths that are weighted and summed in separate power combiners to form two independent subarray main channels (or movable phase centers). In each element channel is a T/R module that has amplitude and phase control. The amplitude control provides the desired low-sidelobe array illumination function and phase-center displacement. The modules utilize phase shifters that steer the main beam to a desired angle.

Let

$$\mathbf{W}_A = \left(W_1^A,\ W_2^A,\ \ldots\ ,\ W_N^A\right)^{\mathrm{T}}$$

and

$$\mathbf{W}_B = \left(W_1^B,\ W_2^B,\ \ldots\ ,\ W_N^B\right)^{\mathrm{T}}$$

denote the array-element weight vectors (including quantization and random errors) of phase centers A and B, respectively (superscript T means transpose). To effect phase-center displacement, a portion of each subarray is turned off by applying a large value of attenuation for a group of antenna elements. This action moves the electrical phase center to the center of gravity for the remaining elements.

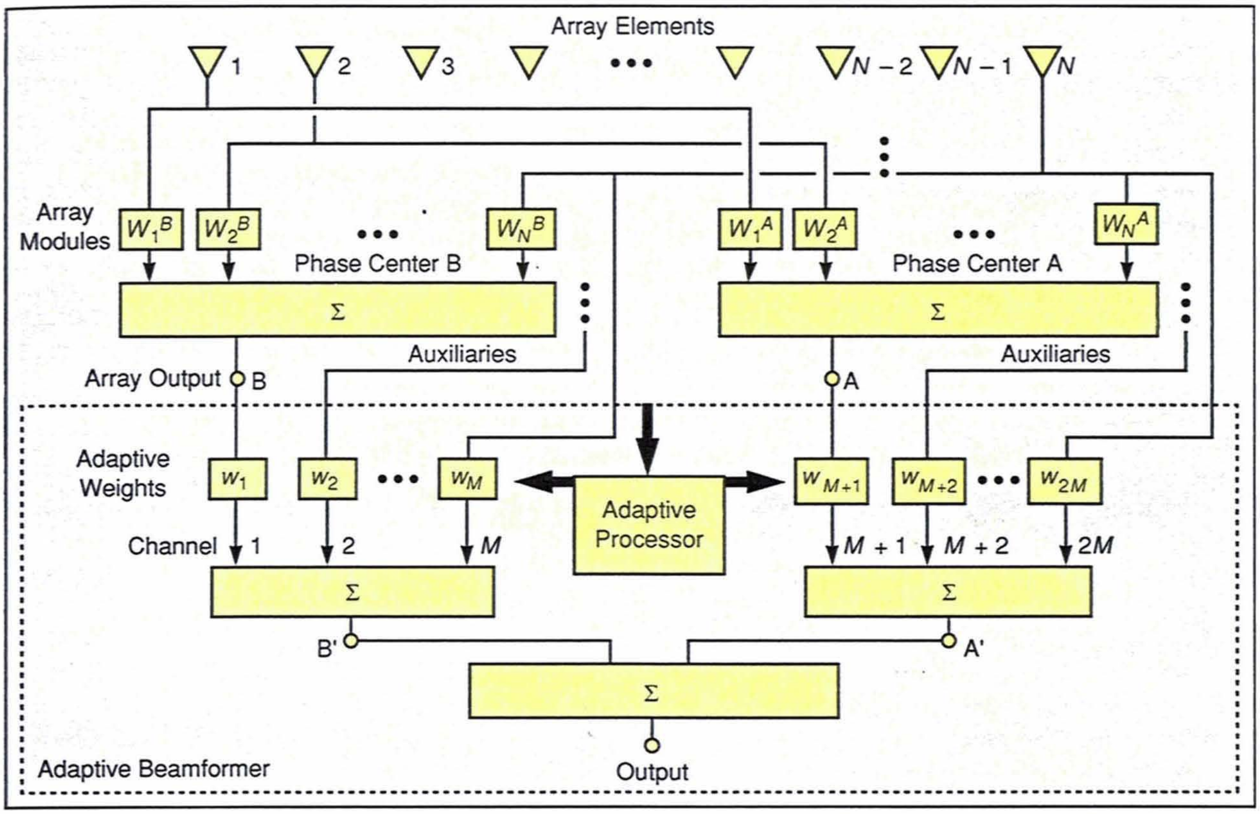

Fig. 8—Adaptive beamformer arrangement for DPCA operation. The output from each antenna element is split into two paths independently weighted with the array modules that contain amplitude and phase control. The outputs of the main channels and auxiliary channels are adaptively weighted to null the interference. The vertical arrow entering the adaptive processor refers to the input data vector consisting of samples of the main and auxiliary channels. The horizontal arrows exiting the adaptive processor refer to the adaptive weight commands. The jamming signals in phase centers A and B are canceled at points A′ and B′, while the clutter is canceled at the final output of the adaptive beamformer.

Thus the effective number of elements actually used to receive signals in phase centers A and B are denoted by N_A and N_B, respectively.

When a wavefront (either planar or spherical) due to the jth source (either clutter or jammer) passes across the array, the result is a set of array-element received voltages denoted by

$$v_1^j,\ v_2^j,\ \ldots\ ,\ v_N^j .$$

Let M be the number of adaptive channels per phase center. For a sidelobe canceler $M = 1 + N_{aux}$ where N_{aux} is the number of auxiliary channels in each phase center. This adaptive system has M degrees of freedom in each phase center and thus a total of $2M$ degrees of freedom for the combined phase centers. For each phase center, the main- and auxiliary-channel voltages are derived from the above set of array received voltages. In this article, ideal adaptive weights (no quantization or random errors) are assumed, with

$$\mathbf{w} = \left(w_1,\ w_2,\ \ldots\ ,\ w_{2M}\right)^{\mathrm{T}}$$

denoting the adaptive-channel weight vector. The fundamental quantities required to characterize the incident field for adaptive nulling purposes are the adaptive-channel cross-correlations.

The cross-correlation R_{mn}^j of the received voltages in the mth and nth adaptive channels, due to the jth source, is given by

$$R_{mn}^j = \mathbf{E}\left(v_m v_n^*\right) \tag{3}$$

where * means complex conjugate and $\mathbf{E}(\cdot)$ means mathematical expectation. (For notational convenience, note that the superscript j in v_m and v_n in Eq. 3 has been omitted.) Since

v_m and v_n represent voltages of the same waveform, but at different times, R^j_{mn} is also called an autocorrelation function.

In the frequency domain, assuming the source has a band-limited white-noise power spectral density, Eq. 3 can be expressed as the frequency average

$$R^j_{mn} = \frac{1}{B}\int_{f_1}^{f_2} v_m(f)\, v_n^*(f)\,\mathrm{d}f \tag{4}$$

where $B = f_2 - f_1$ is the nulling bandwidth. Note that Eq. 4 accounts for the spherical or planar shape of the wavefront.

Let the channel or source covariance matrix be denoted $\mathbf{R}$. If J uncorrelated broadband interference sources exist, then the J-source covariance matrix is the sum of the covariance matrices for the individual sources. Thus

$$\mathbf{R} = \sum_{j=1}^{J} \mathbf{R}_j + \mathbf{I} \tag{5}$$

where $\mathbf{R}_j$ is the covariance matrix of the jth source, and $\mathbf{I}$ is the identity matrix that represents the thermal noise level of the receiver.

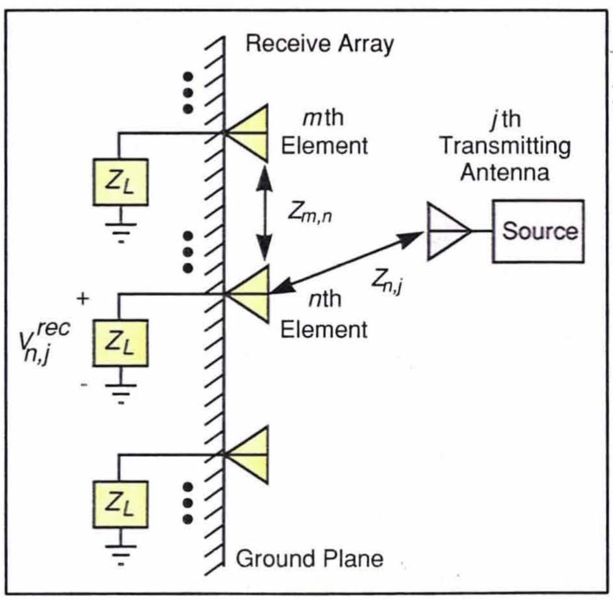

Fig. 9—Receive array and near-field source antenna model. The quantity $Z_{m,n}$ represents the mutual impedance between array elements, while $Z_{n,j}$ represents the mutual impedance between the nth element and the jth transmitting antenna.

Prior to generation of an adaptive null, the adaptive-channel weight vector $\mathbf{w}$ is chosen to maintain a desired quiescent radiation pattern. When undesired signals are present, the optimum set of weights $\mathbf{w}_a$ to form one or more adaptive nulls is computed by

$$\mathbf{w}_a = \mathbf{R}^{-1}\mathbf{w}_q$$

where $\mathbf{w}_q$ is the quiescent weight vector [12]. For a dual-phase-center sidelobe canceler, the quiescent weight vector is chosen to be

$$\mathbf{w}_q = (1, 0, 0, \ldots, -1, 0, 0, \ldots, 0)^{\mathrm{T}}.$$

Thus the main-channel weights are ± 1 and the auxiliary-channel weights are zero.

The output power at the adaptive-array summing junction is given by

$$p = \mathbf{w}^{*\mathrm{T}}\mathbf{R}\mathbf{w} \tag{6}$$

where $^{*\mathrm{T}}$ means complex conjugate transpose. The interference-plus-noise-to-noise ratio, denoted INR, is computed as the ratio of the output power with the interferer present (defined in Eq. 6) to the output power with only receiver noise present; that is,

$$\mathrm{INR} = \frac{\mathbf{w}^{*\mathrm{T}}\mathbf{R}\mathbf{w}}{\mathbf{w}^{*\mathrm{T}}\mathbf{w}}.$$

The adaptive-array cancellation ratio, denoted C, is defined here as the ratio of interference output power after adaption to the interference output power before adaption,

$$C = \frac{p_a}{p_q}. \tag{7}$$

Substituting Eq. 6 into Eq. 7 yields

$$C = \frac{\mathbf{w}_a^{*\mathrm{T}}\mathbf{R}\mathbf{w}_a}{\mathbf{w}_q^{*\mathrm{T}}\mathbf{R}\mathbf{w}_q}.$$

Next, the covariance matrix defined by the elements in Eq. 3 is Hermitian (that is, $\mathbf{R} = \mathbf{R}^{*\mathrm{T}}$). By the spectral theorem, $\mathbf{R}$ can be decomposed in eigenspace as

$$\mathbf{R} = \sum_{k=1}^{2M} \lambda_k \mathbf{e}_k \mathbf{e}_k^{*\mathrm{T}}$$

where λ_k, $k = 1, 2, \ldots, 2M$ are the eigenvalues of $\mathbf{R}$, and $\mathbf{e}_k$, $k = 1, 2, \ldots, 2M$ are the associated eigenvectors of $\mathbf{R}$ [17]. The multiple-source covariance matrix eigenvalues $(\lambda_1, \lambda_2, \ldots, \lambda_{2M})$ are a convenient quantitative measure of the utilization of the degrees of freedom of the adaptive array. Because the identity matrix was added to the covariance matrix, the minimum amplitude that an eigenvalue can have is 0 dB (the receiver noise level). The number of eigenvalues above the receiver noise level directly indicates how many degrees of freedom are used to suppress the undesired signals [13, 18].

Array Antenna/Source Modeling

This section applies the method of moments, already mentioned on p. 25, to compute the array-element received voltages (given in Eq. 3) due to near-field or far-field sources. The far-field formulation in this article is similar to the formulation considered by I.J. Gupta and A.A. Ksienski [19]. Assume that each element is terminated in a known load impedance Z_L (Fig. 9). Let $v_{n,j}$ represent the open-circuit voltage in the nth array element due to the jth source. The jth source can denote either the CW calibrator—a movable source probe for sampling the near-field radiation pattern—or one of the jammer or clutter sources. Next, let $\mathbf{Z}$ be the open-circuit mutual-impedance matrix for the N-element array. The array elements are assumed to be dipoles over an infinite ground plane. The array received-voltage matrix, denoted $\mathbf{v}_j^{\text{rec}}$, due to the jth source, can be expressed as

$$\mathbf{v}_j^{\text{rec}} = Z_L\left[\mathbf{Z} + Z_L\mathbf{I}\right]^{-1}\mathbf{v}_j \qquad (8)$$

[20]. In Eq. 8 the nth element of $\mathbf{v}_j$ is computed, for near-field sources, by the relation

$$v_{n,j} = i_j Z_{n,j}$$

where i_j is the terminal current for the jth source and $Z_{n,j}$ is the open-circuit mutual impedance between the jth source and the nth array element. For thin-wire array antenna elements, the moment-method expansion and testing functions are assumed to be sinusoidal. The above open-circuit mutual impedances are computed on the basis of modified subroutines from a well-known moment-method computer code [21]. In the modified subroutines, double-precision computations are necessary to evaluate $Z_{n,j}$ for the jth interferer. For far-field sources, $v_{n,j}$ is evaluated by assuming plane-wave incidence. The main-channel output is computed by using $\mathbf{W}_A^{*T}\mathbf{v}_{Aj}$ for receive phase center A and $\mathbf{W}_B^{*T}\mathbf{v}_{Bj}$ for receive phase center B, where $\mathbf{v}_{Aj}$ and $\mathbf{v}_{Bj}$ are the received voltages of phase center A and B, respectively, due to the jth source.

As mentioned earlier, each phase center of the array is initially calibrated (phase focused) by a CW radiating dipole. To accomplish this calibration numerically, after computation of the CW received voltage the receive-array weight vector $\mathbf{W}_A$ (or $\mathbf{W}_B$) has its phase commands set equal to the conjugate of the corresponding received phases. Receive-antenna radiation patterns are obtained by scanning (moving) a dipole with half-length l in either the far-field or near-field region and computing the antenna response. Far-field receive patterns are computed by using a $\hat{\theta}$-polarized dipole source at infinity to generate plane-wave illumination of the array. The open-circuit voltage is then set equal to the amplitude and phase of the incident far-field wavefront. For a far-field source, the incident wavefront amplitude is a constant and the phase varies linearly from element to element. The coordinates (x, y, z) specify a near-field point in front of the test antenna. Principal plane near-field radiation pattern cuts (versus angle) are obtained by computing the near field on the line $(x, 0, z_o)$ with the relation $\theta(x) = \tan^{-1}(x/z_o)$. The near-field source is an $\hat{x}$-polarized dipole with half-length l. Let $v_x^{\text{NF}}(\theta)$ denote the voltage received by the array due to the x-directed near-field dipole, and let $p_\theta(\theta)$ denote the $\hat{\theta}$ component of the dipole probe pattern. Then the probe-compensated array near-field received pattern is expressed as

$$E_\theta(\theta)^{\text{NF}} = \frac{v_x^{\text{NF}}(\theta)}{p_\theta(\theta)} \qquad (9)$$

where the value

$$p_\theta(\theta) = \frac{\cos(\beta l \sin\theta) - \cos(\beta l)}{\cos\theta}. \qquad (10)$$

The propagation constant β is $2\pi/\lambda$.

The array received-voltage matrix for the jth source (denoted $\mathbf{v}_j^{\text{rec}}$) is computed at K frequencies across the nulling bandwidth. To obtain the received voltages

$$\mathbf{v}_j^{\text{rec}}(f_1),\ \mathbf{v}_j^{\text{rec}}(f_2),\ \ldots,\ \mathbf{v}_j^{\text{rec}}(f_K)$$

the impedance matrix $\mathbf{Z}$ is computed at K frequencies and the system of equations given by Eq. 8 is solved at each frequency. The interference covariance matrix elements are computed by numerically integrating Eq. 4 according to Simpson's rule. For multiple sources, the covariance matrix is evaluated by using Eq. 5. Adaptive-array radiation patterns are computed by superimposing the quiescent radiation pattern with the weighted sum of auxiliary-channel received voltages.

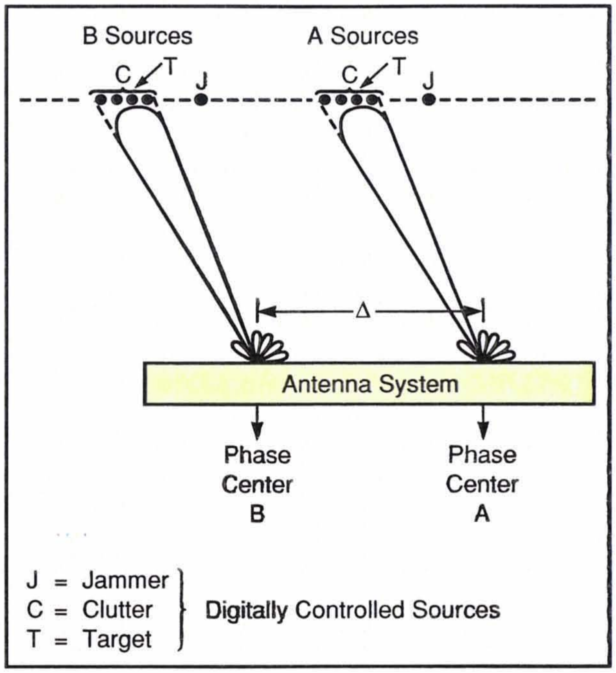

Fig. 10—Near-field source positioning for a displaced phase-center antenna. Two sets of sources, "A" and "B," are used one set at a time to illuminate the test antenna.

DPCA Near-Field Source Distribution

Figure 10 shows the position of near-field sources for two-phase-center DPCA operation. Two sets of sources exist, one set for phase center A and one set for phase center B. Multiple clutter sources are distributed across the main beam of both phase centers. The figure also shows a desired target signal embedded within the clutter signals. Jammer signals are assumed to radiate from antennas located within the sidelobe region. As mentioned before, the clutter is correlated between phase centers A and B. As an example, denote the first clutter source in phase center A as $C_{A1}(\theta_1)$ and the first clutter source in phase center B as $C_{B1}(\theta_1)$. Clearly, in theory $C_{A1}(\theta_1)$ equals $C_{B1}(\theta_1)$. Similar equalities exist for the remaining clutter sources. To achieve this correlation in an experimental configuration requires digitally controlled arbitrary-waveform generators. These signal generators can also create the jammers and desired target signals. The two sets of sources must be operated during different time intervals separated by the radar PRI delay. Thus, for example, a measurement of the phase center A signals is performed with only the "A" group of sources radiating. The next measurement (one PRI later) is for the phase center B signals with only the "B" group of sources radiating. This switching is implemented by using timing and control, as suggested earlier in Fig. 2.

The near-field source antennas do not interact through mutual coupling in such a way that the adaptive nulling performance is modified. For example, with one source radiating, the surrounding source antennas represent possible multipath. The near-field sources are known to couple, but this coupled interference does not influence the adaptive weights, provided that the coupled signal is reradiated and received at below the receiver noise level. The multipath contribution between two antennas (one radiating and the other passively terminated in a load) is accurately computed as follows. Let I_1 be the terminal current generated on the active source antenna. Similarly, let I_2 denote the parasitic current generated on the

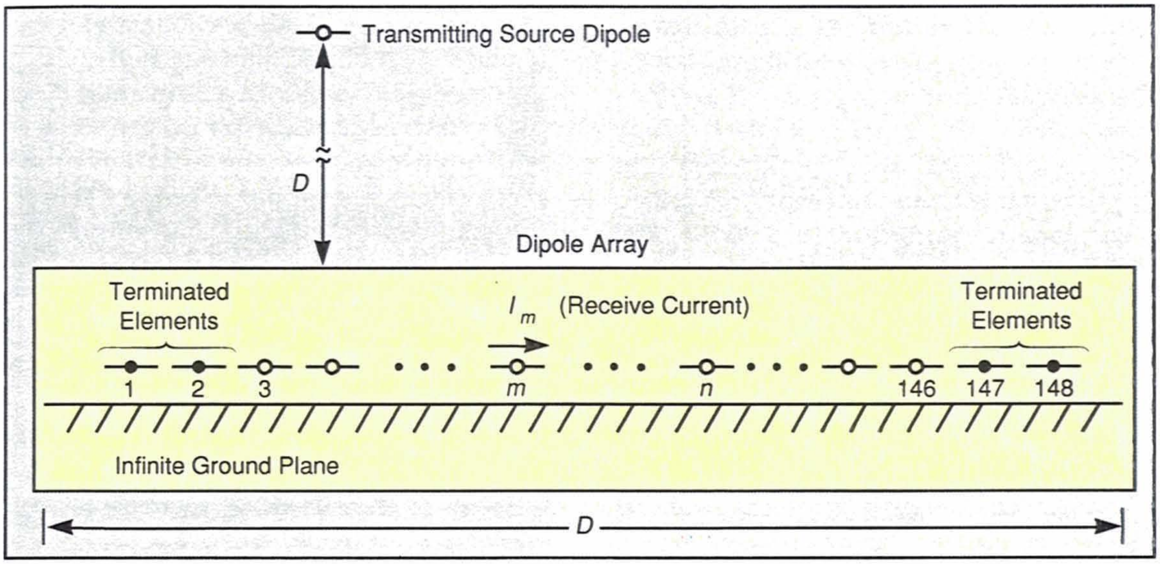

Fig. 11—Geometry for dipole receive array and dipole source antenna. The transmitting source antenna represents clutter, jammer, the target, and noise.

passive antenna. From circuit theory the ratio of the parasitic current to active current is given by

$$\frac{|I_2|}{|I_1|} = \frac{|Z_{21}|}{|Z_{22} + Z_L|} \tag{11}$$

where Z_{21} is the open-circuit mutual impedance between the two antennas, Z_{22} is the self-impedance of the passive antenna, and Z_L is the load impedance of the passive antenna. Clearly, a small value of mutual impedance is desired. Equation 11 will be used later to verify that the mutual coupling between source antennas is sufficiently small for a particular near-field source configuration. An important point to be stressed here is that mutual coupling between source antennas in a particular near-field test configuration needs to be carefully evaluated. However, with proper source antenna design, and judicious placement of anechoic material between source antennas, mutual coupling should not be a problem.

Near-Field/Far-Field Simulations

This section analyzes a specific adaptive DPCA array and demonstrates the equivalence between near-field clutter and jammer suppression and far-field clutter and jammer suppression. Consider a corporate-fed phased-array 16-m antenna that consists of a single row of receive dipole elements. The array, which has a total of $N = 148$ elements with two elements at each end used as passive terminations, has 144 active receive antenna elements. The antenna elements are one-half-wavelength-long electrically thin dipoles that are center fed and spaced one-quarter wavelength above an infinite ground plane (Fig. 11). The center frequency is chosen to be 1.3 GHz (L-band) and the interelement spacing is 10.922 cm, or 0.473 wavelengths. Thus the active portion of the array spans 15.61 m. The output from each active receive antenna element is divided into two paths to form two independent phase centers. The T/R modules are chosen to have 5 bits of amplitude and phase control with rms errors of 0.3 dB and 3.0°. The load impedance Z_L is assumed to be 50 Ω resistive at each array element.

The near-field test distance z is chosen to be 15.61 m, which corresponds to one active receive aperture diameter. Seven auxiliary channels, randomly selected from the element outputs of one of the phase centers, form a multiple-sidelobe canceler configuration. This random pattern repeats in the second phase center. Since the value of N_{aux} is 7 in each phase center, the total number of degrees of freedom is 16. The channel covariance matrix is dimensioned 16×16 and has 16 eigenvalues. The receiver

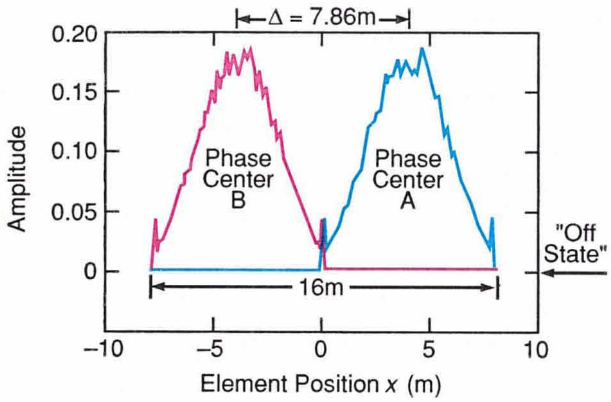

Fig. 12—Simulated DPCA illumination functions for the 16-m linear test array. The phase-center displacement Δ is created by turning off the left half of the array for phase center A and the right half of the array for phase center B.

bandwidth (also called the nulling bandwidth) is 1 MHz. The auxiliary channels are attenuated by 20 dB to have a signal output power comparable to the main channels. In a practical radar, auxiliary-channel attenuation will be implemented to keep the dynamic range of signals within the limits of the adaptive nulling receiver.

Let the array illumination be chosen to

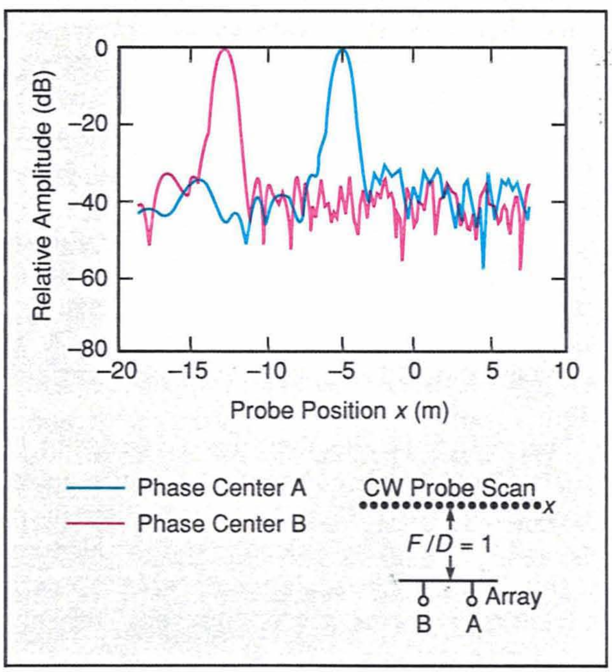

Fig. 13—Simulated near-field probe scan at one-aperture-diameter test distance for the DPCA 16-m linear test array. The source frequency is 1.3 GHz and the receive-array scan angle is −30°.

synthesize a −40-dB uniform-sidelobe-level Chebyshev radiation pattern (in the absence of T/R module errors) with a scan angle θ_s equal to −30°. Assume that the phase centers are fully split apart, so that the effective number of receive elements per phase center (N_A and N_B) is one-half of 144, or 72. This number gives a phase-center separation of 7.86 m. Figure 12 shows the subarray amplitude illumination function for phase centers A and B. The expected random amplitude error of the T/R

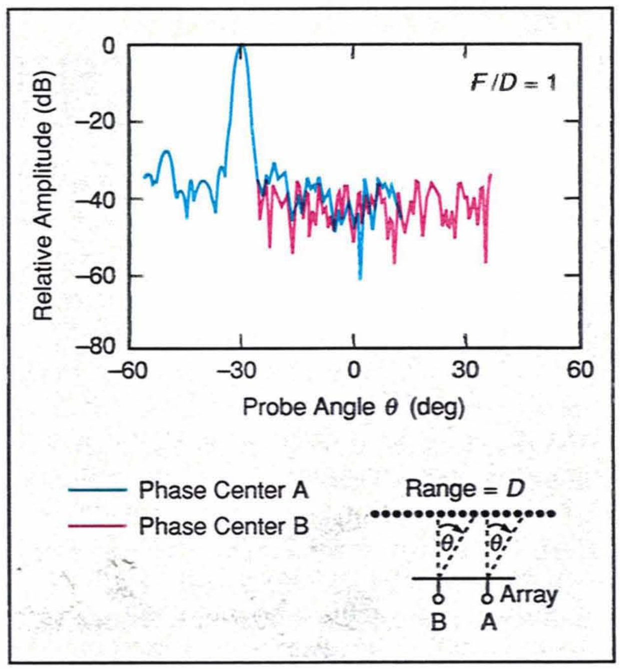

Fig. 14—Near-field radiation patterns at one-aperture-diameter test distance for phase centers A and B, as a function of observation angle. The patterns are computed from Eqs. 9 and 10 by using the simulated near-field data in Fig. 13.

modules makes the illumination functions slightly different from one another. Notice how each illumination function is equal to zero over 7.86 m. This illumination shifts the apparent phase center by 3.93 m to the left of the antenna center for phase center B and 3.93 m to the right of the antenna center for phase center A.

To phase-focus the DPCA array in the near field to the distance z_s = 15.61 m and angle θ_s = −30° (with respect to each phase center), a CW radiating dipole source is positioned at x = −12.95 m for phase center B and at

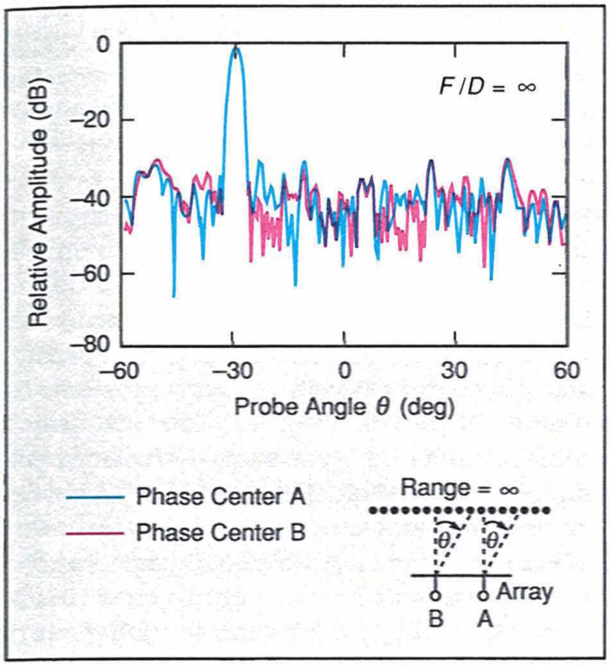

Fig. 15—Simulated far-field radiation pattern for the DPCA 16-m linear array. The focal distance and observation distance are both set to infinity.

x = –5.09 m for phase center A. To focus the subarrays, the conjugate of the moment-method-calculated element phases is applied to the receive modules. The CW source is scanned across 26.29 m and the array output is computed at uniformly spaced probe positions. Figure 13 shows the resulting near-field received amplitude distribution for both phase centers. Notice that the peak amplitudes occur at the desired locations. The main beams are fully separated so that one phase center has a peak when the other phase center has a sidelobe. While the test distance is specified as one aperture diameter for the full length of the array, the test distance effectively appears to be two subarray diameters for the displaced phase centers. Figure 14 shows the near-field data replotted as a function of angle with respect to each phase center. The near-field main beams of phase centers A and B are clearly well matched as desired in a DPCA system. Because of phase-center displacement, the near-field patterns cover different angular sectors. Figure 15 shows the corresponding far-field radiation patterns of phase centers A and B. A good main-beam match is also apparent in this figure.

Figure 16 compares near-field and far-field radiation patterns. Figures 16(a) and 16(b) show the radiation patterns for phase centers B and A, respectively. The near-field main beam agrees with the far-field main beam down to –20 dB. Amplitude calibration can compensate for a defocusing of the near-field main beam and first sidelobes, as mentioned earlier. Although the near-field sidelobes do not match the far-field

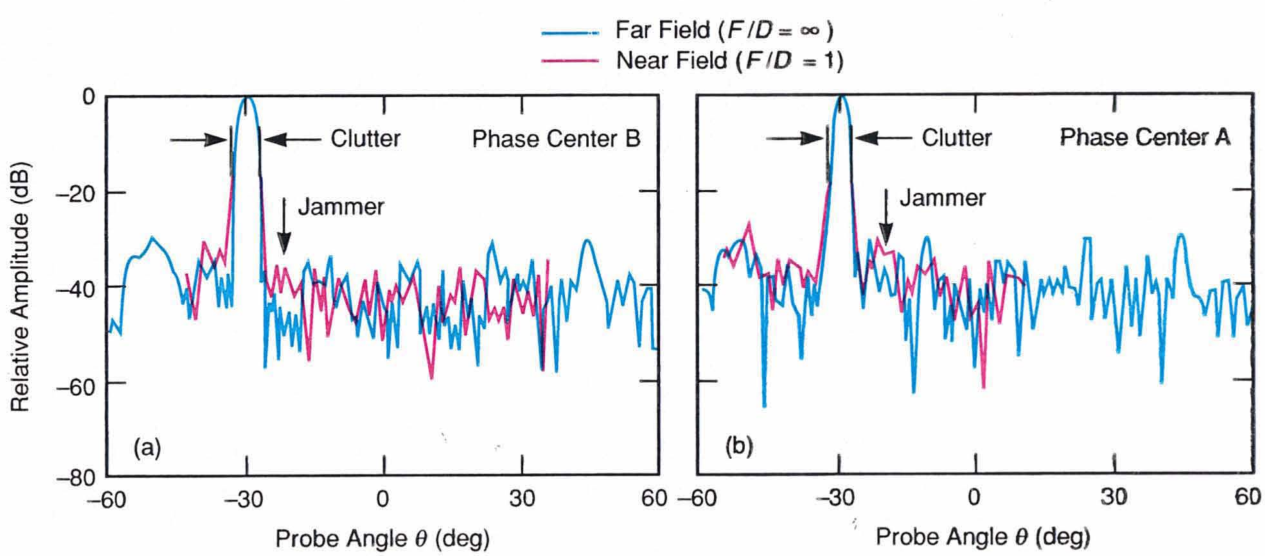

Fig. 16—Comparison of simulated near-field and far-field DPCA radiation patterns (before adaptive nulling) previously shown in Figs. 14 and 15, respectively. The (a) phase center B radiation patterns and (b) phase center A radiation patterns establish the quiescent conditions for the adaptive antenna.

sidelobes on a point-by-point basis, the average sidelobe levels are equal.

When proper quiescent conditions are established, seven clutter sources are uniformly distributed across the main beam of both near-field and far-field patterns. For this dual-phase-center example, seven clutter sources exist per phase center. In each phase center, all sources are assumed to have equal power and all sources are uncorrelated. Note that equal-power sources are chosen for convenience. The sources are distributed in angle over a 5° sector centered at the beam peak, and they cover the main beam down to −20 dB. The total power that these sources produce in one phase center equals 40 dB relative to receiver noise. An increase in the number of clutter sources beyond seven does not significantly influence the adaptive nulling results that follow. Finally, let one jammer be positioned at $\theta = -20°$ to produce an output power for the combined phase centers of 50 dB above noise.

As mentioned earlier, mutual coupling among near-field signal sources can be an important consideration. In the current example, since the sidelobe jammer power is large the coupling between the radiating jammer antenna and a clutter antenna is the most important case to consider. The sidelobe level at the jammer position is approximately −35 dB down from the main-beam peak. The main-beam level at the nearest clutter antenna position is −20 dB. Thus a parasitically generated jammer signal at the clutter antenna is effectively increased by 15 dB at the test antenna because of the pattern directivity increase. Without the contribution of mutual coupling, the parasitic jammer power in the main beam would be 65 dB above noise. The parasitic jammer current at the clutter antenna is computed by using Eq. 11. The self-impedance of a one-half-wavelength clutter dipole is $Z_{22} = 73 + j42\ \Omega$. The separation between the jammer and the nearest clutter antenna is approximately 10λ. For this spacing, the mutual impedance is computed to be $Z_{21} = -0.03748 - j0.000618\ \Omega$. Substituting these values and the load impedance ($Z_L = 50\ \Omega$) into Eq. 11 yields

$$\frac{|I_2|}{|I_1|} = 0.000289.$$

In decibels, the parasitic jammer current is down by −71 dB. The parasitic jammer signal is then the difference between 65 dB and 71 dB, or −6 dB below receiver noise. According to

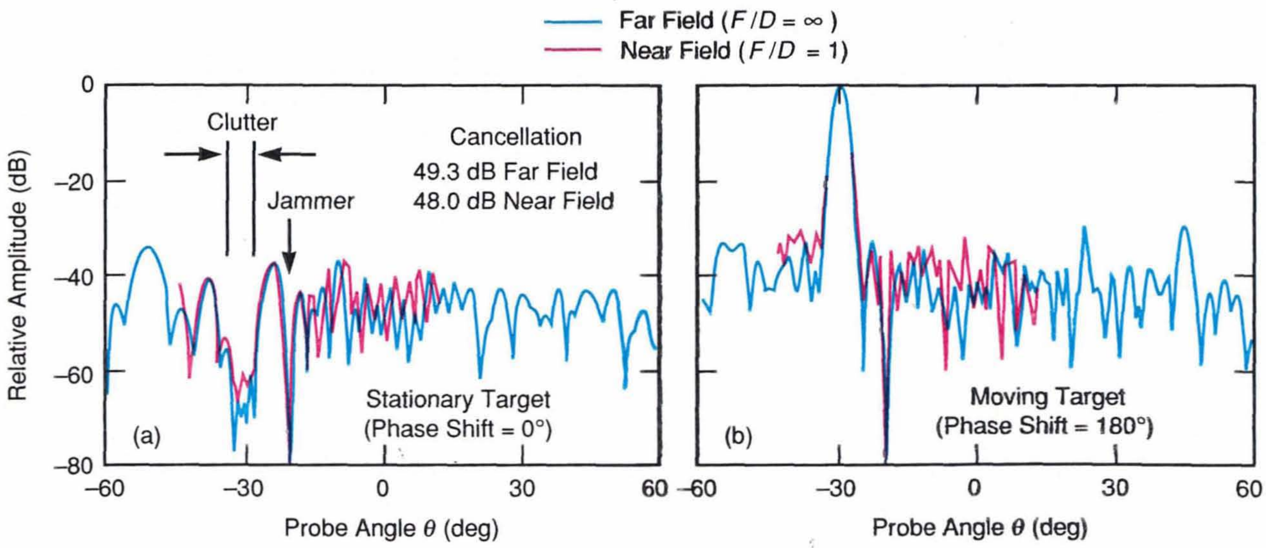

Fig. 17—Adapted radiation patterns for the combined phase centers of the DPCA 16-m linear array for the (a) stationary target and (b) moving target. The near-field simulation is at a test distance of one aperture diameter and the far-field simulation is at a test distance of infinity. Seven white-noise clutter sources are distributed uniformly across the main beam, and one white-noise jammer is in a sidelobe. The nulling bandwidth is 1 MHz.

theoretical simulations, this power level does not affect the computation of the adaptive weights.

For the signal environment, the covariance matrix was computed and the adapted weights were derived and then applied to cancel the interference. Figure 17 shows the near-field and far-field adapted radiation patterns. In Fig. 17(a), both the clutter and jammer are clearly suppressed by the pattern nulls, and the patterns are very similar. The total cancellation of jamming and clutter power is 48.0 dB in the near field and 49.3 dB in the far field. As the amount of cancellation is large, this small difference (1.3 dB) is insignificant. The radiation patterns in Fig. 17(a) show a stationary target whose signal is effectively canceled because of zero phase shift in one PRI. In contrast, a received signal from a moving target that produces a 180° phase shift in one PRI sees the antenna radiation pattern shown in Fig. 17(b), where full antenna gain is available in the main-beam direction. Finally, Figure 18 shows a plot of the covariance matrix eigenvalues. A total of eight eigenvalues above receiver noise indicates that eight degrees of freedom are consumed. The near-field and far-field eigenvalues are in good agreement over a large dynamic range. By taking all of the above results into consideration, we can now state that, for all practical purposes, near-field nulling is equivalent to far-field nulling.

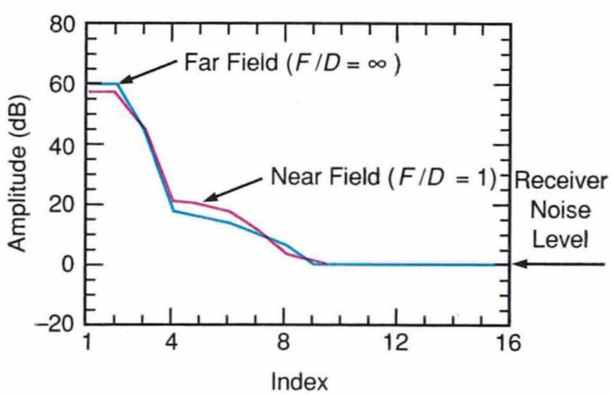

Fig. 18—Covariance matrix eigenvalues for near-field and far-field source distributions. Eigenvalues 1 to 8 are above the receiver noise level and represent the consumption of eight degrees of freedom.

Conclusion

A theory for analyzing sources radiating in the near field of an adaptive radar system is developed. Conventional phase focusing of an array is used to create antenna far-field pattern conditions in the near-field region. Clutter sources are distributed across the main beam of the focused antenna pattern, and jammers are positioned within the sidelobes. The method of moments is used to analyze a displaced phase-center antenna linear array with near-field and far-field clutter and jamming. Focused near-field adaptive nulling is shown to be equivalent to conventional far-field adaptive nulling. The near-field range distance can be one aperture diameter, which opens the possibility for indoor anechoic chamber testing. Thus a radar system designed for far-field conditions can potentially be evaluated by using near-field sources. This technique is particularly attractive for space-based radar systems for which prelaunch ground testing is desirable. With this method, integrated testing of a phased-array antenna, receiver, and adaptive signal processor can be performed. Array calibration, antenna radiation patterns, adaptive cancellation, and target detection can be verified. Experimental verification of this technique is currently under investigation.

Acknowledgements

Initial development of the near-field testing technique was encouraged by V. Vitto and H. Kottler, and their support is appreciated. Technical discussions with G.N. Tsandoulas, R.W. Miller, J.R. Johnson, H.M. Aumann, F.G. Willwerth, E.J. Kelly, D.H. Temme, and S.C. Pohlig were valuable in the development of this work. The software support of S.E. French is also appreciated.

References

1. L.J. Cantafio, ed., *Space-Based Radar Handbook* (Artech House, Dedham, MA, 1989).
2. E.J. Kelly and G.N. Tsandoulas, "A Displaced Phase Center Antenna Concept for Space Based Radar Applications," *IEEE 16th Ann. Electron. and Aerospace Conf. and Expo., Washington, DC, 19–21 Sept.*

1983, p.141.
3. G.N. Tsandoulas, "Space-Based Radar," *Science* **237,** 257 (1987).
4. A.D. Yaghjian, "An Overview of Near-Field Antenna Measurements," *IEEE Trans. Antennas Propag.* **AP-34,** 30 (1986).
5. A.J. Fenn, F.G. Willwerth, and H.M. Aumann, "Displaced Phase Center Antenna Near Field Measurements for Space-Based Radar Applications," *Phased Arrays 1985 Symp. Proc., Bedford, MA, 15–18 Oct. 1985*, p. 303, RADC-TR-85-171, ADA-169316.
6. C.H. Walter, *Traveling Wave Antennas* (Dover, New York, 1970), p. 38.
7. R.C. Johnson, H.A. Ecker, and R.A. Moore, "Compact Range Techniques and Measurements," *IEEE Trans. Antennas Propag.* **AP-17,** 568 (1969).
8. A.J. Fenn, "Theory and Analysis of Near-Field Adaptive Nulling," *1986 IEEE AP-S Symp. Digest, Vol. 2* (IEEE, New York, 1986), p. 579.
9. A.J. Fenn, "Evaluation of Adaptive Phased Array Antenna Far-Field Nulling Performance in the Near-Field Region," *IEEE Trans. Antennas Propag.* **AP-38,** 173 (1990)
10. A.J. Fenn, "Theoretical Near-Field Clutter and Interference Cancellation for an Adaptive Phased Array Antenna," *1987 IEEE AP-S Symp. Digest, Vol. 1* (IEEE, New York, 1987), p. 46.
11. A.J. Fenn, "Moment Method Analysis of Near-Field Adaptive Nulling," *IEE 6th Intl. Conf. on Antennas and Propagation, ICAP 89, Coventry, UK, 4–7 Apr. 1989*, p. 295.
12. R.A. Monzingo and T.W. Miller, *Introduction to Adaptive Arrays* (Wiley, New York, 1980), p. 253.
13. J.T. Mayhan, "Some Techniques for Evaluating the Bandwidth Characteristics of Adaptive Nulling Systems," *IEEE Trans. Antennas Propag.* **AP-27,** 363 (1979).
14. W.E. Scharfman and G. August, "Pattern Measurements of Phased-Arrayed Antennas by Focusing into the Near Zone," *Phased Array Antennas (Proc. of the 1970 Phased Array Antenna Symp.)*, eds. A.A. Oliner and G.H. Knittel (Artech House, Dedham, MA, 1972), p. 344.
15. W.L. Stutzman and G.A. Thiele, *Antenna Theory and Design* (Wiley, New York, 1981), p. 306.
16. H.M. Aumann and F.G. Willwerth, "Synthesis of Phased Array Far-Field Patterns by Focusing in the Near-Field," *Proc. of the 1989 IEEE Natl. Radar Conf. Dallas, TX, 29–30 Mar. 1989*, p. 101.
17. G. Strang, *Linear Algebra and Its Applications* (Academic Press, New York, 1976), p. 213.
18. A.J. Fenn, "Maximizing Jammer Effectiveness for Evaluating the Performance of Adaptive Nulling Array Antennas," *IEEE Trans. Antennas Propag.* **AP-33,** 1131 (1985).
19. I.J. Gupta and A.A. Ksienski, "Effect of Mutual Coupling on the Performance of Adaptive Arrays," *IEEE Trans. Antennas Propag.* **AP-31,** 785 (1983).
20. A.J. Fenn, "Moment Method Analysis of Near-Field Adaptive Nulling," *Technical Report 842*, Lincoln Laboratory (7 Apr. 1989), AD-A208-228.
21. J.H. Richmond, "Radiation and Scattering by Thin-Wire Structures in a Homogeneous Conducting Medium (Computer Program Description)," *IEEE Trans. Antennas Propag.* **AP-22,** 365 (Mar. 1974).

ALAN J. FENN is a staff member in the Space Radar Technology group, where his research is in the development of near-field testing techniques for adaptive radar systems. He has a B.S. degree from the University of Illinois at Chicago, and M.S. and Ph.D. degrees from Ohio State University, all in electrical engineering. Before coming to Lincoln Laboratory in 1981, Alan worked for Martin Marietta Aerospace Corporation in Denver, Colo. He is currently an associate editor in the area of adaptive arrays for the *IEEE Transactions on Antennas and Propagation*.